APPLICATION OF A SINTERING MODEL TO THE ANALYSIS OF TES SPECTRA OF THE SEASONAL CAPS. J. Eluszkiewicz[1] and T. N. Titus[2], [1]Atmospheric and Environmental Research, Inc., 131 Hartwell Ave., Lexington, MA 02421, jel@aer.com, [2]U.S. Geological Survey, 2255 North Gemini Dr., Flagstaff, AZ 86001, ttitus@usgs.gov.

Introduction: There is abundant evidence that large portions of the seasonal CO_2 deposits in the polar regions of Mars form a solid slab rather than a fluffy frost. Flashes from the polar caps, suggestive of specular reflection, have been frequently sighted by amateur astronomers [1]. The presence of low−porosity slabs is also indicated by the NIR spectroscopic measurements of the caps [2,3], Viking/IRTM data [4], and the fact that the southern residual cap can be distinguished in visible images when the seasonal frost is present [5]. Most recently, TES data acquired during southern spring led to the identification of a "Cryptic" region near the South Pole characterized by a spectroscopic grain size in the thermal IR as large as 1 meter [6]. An analysis of the TES spectra acquired during northern winter also revealed that slab ice dominates the seasonal CO_2 deposits, at least at latitudes outside of the polar night [7]. Pressureless sintering has been proposed as the physical mechanism for the seasonal formation of semitransparent CO_2 slabs [8]. According to the sintering model, the slabs are polycrystalline, with the size of individual crystals smaller than 10 μm, and the long visible/IR path lengths result from the elimination of voids between crystals. In this presentation we will describe initial results from an application of the sintering model aimed at explaining the time variations detected in the TES spectra of the caps.

Microphysical State of Seasonal Frosts Inferred from TES Data: Slab ice can be distinguished from porous frost by the shape of the 25−μm band in the TES spectra, with small band depth BD_{25} indicative of low porosity. BD_{25} is defined as the fractional drop in the measured band radiance relative to the expected blackbody radiance at the brightness temperature of adjacent continua [6]. Two sample TES spectra of the southern seasonal cap with small and large BD_{25} are shown in . The interpretation of low values of BD_{25} as indicative of a slab−like texture has strong physical basis, with zero BD_{25} corresponding to Fresnel reflection [6]. The identification of high BD_{25} (i.e., low emissivity) with high porosity also appears plausible and is supported by experimental data on the emissivity of other materials in various stages of densification [9]. However, a rigorous derivation of the relationship between emissivity and porosity φ does not appear to exist and we will rely on a heuristic argument in order to relate BD_{25} to φ (see below).

TES spectra also provide indication of time evolution in the microphysical state of seasonal CO_2 deposits. A particularly well−suited location for studying the evolution of BD_{25} are the polar rings corresponding to the northern− and southernmost latitudes of the MGS orbit (87°), which are characterized by almost daily repeat coverage. In we plot BD_{25} as a function of time and longitude in the rings. Both rings are covered by slab ice (low BD_{25}, purple) during prolonged periods in fall and winter. In the zonal band 0−60°W in the southern ring during the MGS first southern winter, the slab appears to form from an initial state of higher BD_{25} (*c*). The subsequent evolution from high to low BD_{25} proceeds on a seasonal time scale (several tens of sols). At other locations in the southern ring, the low values of BD_{25} exhibit little variation with time (e.g., the zonal band 80−100°W in *c* and most longitudes in *b*). This suggests that at those locations the slab may have formed simultaneously with or shortly after frost deposition. In the north, the seasonal evolution towards low BD_{25} is frequently interrupted by the episodic appearance of high BD_{25} values (the so−called "cold spots"). The time scale for the disappearance of cold spots is much shorter, on the order of several sols. Also noticeable in the north are extended periods of large and/or increasing BD_{25}, which appear inconsistent with a sintering−driven metamorphism and point out to the existence of other physical processes affecting BD_{25} (e.g., fracturing, dust contamination). In view of these processes, the sintering model can only provide an end−member scenario for the evolution of BD_{25} and it is likely to be refined in future work.

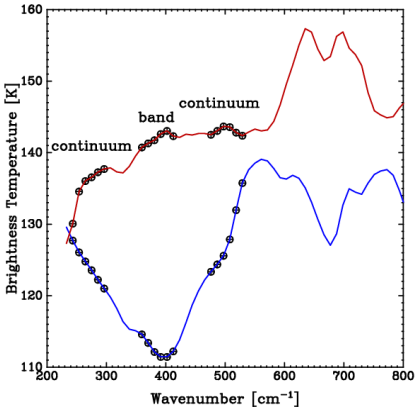

Figure 1: Examples of TES spectra of the southern cap with small and large BD_{25} (red and blue, respectively).

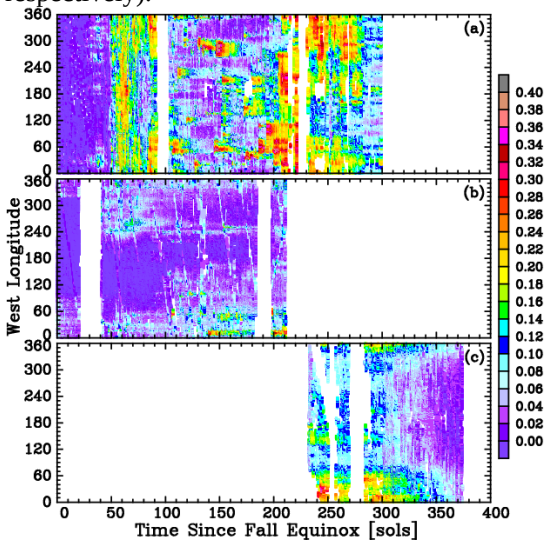

Figure 2: Evolution of BD_{25}: *(a)* northern polar ring in fall and winter (L_s = 180−360°), *(b)* southern polar ring in fall and early winter (L_s = 0−98°), and *(c)* southern polar ring in winter (L_s = 107−180°).

Sintering Model: Sintering is driven by the thermodynamic constraint of minimum surface energy and the attendant evolution of porosity φ can be calculated using kinetic rate equations involving temperature, grain radius *r*, solid−state diffusivities, and surface tension [8]. In order to match the observed evolution of BD_{25} with the evolution of φ predicted by the sintering model, BD_{25} will be related to φ via the concept of mean grain size $\overline{a}$. In past work on the optical properties of the martian polar caps based on Mie theory [6,10], the grain size has been identified as the physical size of spherical grains underlying this approach, leading to a functional relationship $BD_{25} = BD_{25}(\overline{a})$. For illustrative purposes, we will assume $BD_{25} \sim \overline{a}^{-1}$. However, in a sintering medium the concept of distinct grains is no longer valid and the "grain size" $\overline{a}$ represents in this case the mean distance between scattering centers. In a porous medium, scattering occurs predominantly at grain/pore interfaces and consequently we expect $\overline{a}$ on dimensional grounds to be on the order of the ratio (volume)/(pore surface area). In the sintering model, this ratio is inversely proportional to Γ, where

$$\Gamma(\varphi) = \frac{(1-\varphi_o)\varphi(1+\varphi_o-\varphi)}{(1-\varphi)\varphi_o}$$

(1) The two assumptions $BD_{25} \sim \overline{a}^{-1}$ and $\overline{a} \sim \Gamma^{-1}(\varphi)$ give the result $BD_{25} \sim \Gamma(\varphi)$. BD_{25} will be normalized by its maximum value BD_{25}^{max}, i.e., we will assume $BD_{25} = BD_{25}^{max}\Gamma(\varphi)$ [note that Γ(φ) in Equation (1) is normalized, i.e., it varies from 1 to 0 as φ varies between the uncompressed value φ_o and 0]. Clearly, this method of establishing the relationship between BD_{25} and φ is rather crude, but it should be adequate if the interest is in comparing time scales, rather than predicting the detailed evolution of BD_{25}. shows the evolution of BD_{25}/BD_{25}^{max} in a section of the southern ring and compares it with the evolution of Γ computed for r = 10 μm and assuming different pre−exponential factors for lattice diffusion (the other material parameters are as in [8]).

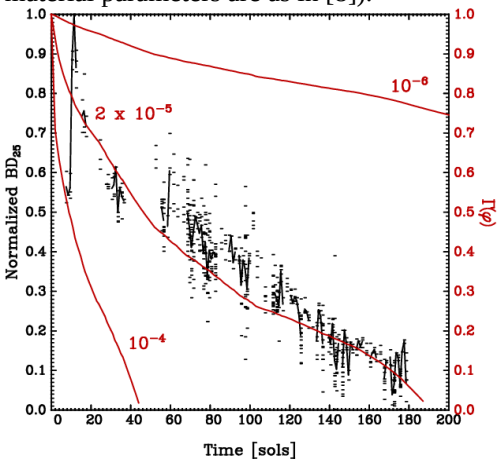

Figure 3: Evolution of BD_{25} in the zonal band 30−40°W in the southern polar ring during the first southern winter of MGS mapping phase (time is counted from L_s = 107°). The red curves represent evolutions of Γ(φ) computed in the sintering model and are labeled by the assumed value of the pre−exponential factor for the lattice diffusion coefficient (in $m^2 s^{-1}$).

Implications: This analysis will produce a physically based parameterization of seasonal frost metamorphism for application in models of the energy budget of the caps and of the general circulation of the martian atmosphere. In addition, it will provide a testbed for theories of frost metamorphism on other planetary bodies, including Triton, Pluto, and Io. This analysis has the potential to increase the predictive accuracy of surface characteristics of Mars from orbit and it might be relevant to the design of future missions to the martian polar regions by shedding light on the mechanical properties of potential landing sites.

References: [1] Beish J. D. (1991) personal communication. [2] Moroz V. I. (1964) *Sov. Astron. 8*, 273. [3] Calvin W. M. (1990) *JGR, 95*, 14,743. [4] Paige D. A. et al. (1995) *BAAS, 27*, 1098. [5] James P. B. et al. (1979) *JGR, 84*, 2889. [6] Kieffer H. et al. (2000) *JGR, 105*, 9653. [7] Titus T. et al. (2001) *JGR* (in press). [8] Eluszkiewicz J. (1993) *Icarus, 103*, 43. [9] Adissin A. et al. (1977) *Trans. J. Br. Ceram. Soc., 76*, 17. [10] Hansen G. B. (1999) *JGR, 104*, 16,471.